



# Hemodynamics alteration in patient-specific dilated ascending thoracic aortas with tricuspid and bicuspid aortic valves

Raja Jayendiran<sup>a</sup>, Salvatore Campisi<sup>b</sup>, Magalie Viallon<sup>c,d</sup>, Pierre Croisille<sup>c,d</sup>, Stéphane Avril<sup>a,\*</sup>

<sup>a</sup> Mines Saint-Étienne, Université de Lyon, INSERM, U1059 SaInBioSE, F-42023 Saint-Étienne, France

<sup>b</sup> Department of Cardiovascular Surgery, University Hospital of Saint-Étienne, Saint-Étienne, France

<sup>c</sup> Université de Lyon, UJM-Saint-Étienne, INSA, CNRS, UMR 5520, INSERM U1206, CREATIS, F-42023 Saint-Étienne, France

<sup>d</sup> Department of Radiology, University Hospital of Saint-Étienne, Saint-Étienne, France

## ARTICLE INFO

### Article history:

Accepted 8 July 2020

### Keywords:

Aneurysm  
4D flow MRI  
Computational Fluid Dynamics  
Biomechanics  
Tricuspid and Bicuspid aortic Valve

## ABSTRACT

In this paper, we evaluate computationally the influence of blood flow eccentricity and valve phenotype (bicuspid (BAV) and tricuspid (TAV) aortic valve) on hemodynamics in ascending thoracic aortic aneurysm (ATAA) patients. 5 TAV ATAA, 5 BAV ATAA (ascending aorta diameter >35 mm) and 2 healthy subjects underwent 4D flow MRI. The 3D velocity profiles obtained from 4D flow MRI were given as input boundary conditions to a computational fluid dynamics analysis (CFD) model. After performing the CFD analyses, we verified that the obtained time-averaged velocity profiles and flow eccentricity were in good agreement with 4D flow MRI. Then we used the CFD analyses to evaluate the time-averaged wall shear stress (TAWSS) and the local normalized helicity (LNH). We found that the flow eccentricities at the aortic root were not significantly different ( $p > 0.05$ ) between TAV and BAV phenotypes. TAWSS ( $R^2 = 0.697$ ,  $p = 0.025$ ) and absolute LNH ( $R^2 = 0.964$ ,  $p < 0.001$ ) are in good correlation with flow eccentricity. We conclude that eccentricity at the aortic root is a major determinant of hemodynamics patterns in ATAA patients regardless of the aortic valve phenotype.

© 2020 Elsevier Ltd. All rights reserved.

## 1. Introduction

Ascending thoracic aortic aneurysms (ATAAs) are life-threatening pathologies characterized by progressive vessel dilation. It is associated with smooth muscle cell dysfunction, occasional localized inflammatory infiltrates, and severe maladaptive extracellular matrix remodeling which together predisposes the arterial wall to dissection and rupture leading to premature death (Lavall et al., 2012; Azadani et al., 2013; Real et al., 2014; Lasheras, 2007; Pasta et al., 2012). Among the etiology of ATAAs, individuals with a BAV are more vulnerable to ATAA than normal TAV. Recent studies have shown that deficient TAVs also contribute to ATAA progression (Muraru et al., 2016). ATAAs progression is the result of multifactorial effects including genetics or epigenetics expressions, biomechanical (Farzaneh et al., 2018) and altered hemodynamics patterns (Girdauskas et al., 2011).

4D PCMRI (phase-contrast magnetic resonance imaging) also called 4D flow MRI has been commonly used to understand aortic hemodynamics (Simao et al., 2017; Bakhshinejad et al., 2017;

Biglino et al., 2015). Retrograde flows and recirculations were frequently found in BAV subjects using 4D flow MRI and it was shown that they occur at earlier age compared to TAVs (Barker et al., 2010; Barker et al., 2012). Moreover, hemodynamics alterations in BAV usually differ with valve fusion alterations (Bissell et al., 2013). Among hemodynamics alterations, the impact on the wall shear stress (WSS) distribution in the ascending aorta (AA) of BAV patients without concomitant valve or vessel disease is significant compared with TAV subjects (Meierhofer et al., 2012). WSS responsive pathways are known to regulate endothelial function and vessel integrity (Baeyens et al., 2016). In coronary or carotid arteries, the endothelial cells exposed to high, unidirectional wall shear stress maintain a quiescent phenotype, while those exposed to low and/or directional varying WSS are activated, displaying a pro-inflammatory phenotype (Kwak et al., 2014). Although studies related to ATAAs are scarcer, there is enough evidence to highlight essential roles of WSS in ATAA progression (Liu et al., 2014; Condemi et al., 2019; Guzzardi et al., 2015). Helicity of the flow also contributes to aneurysm progression (Youssefi et al., 2018; Pirola et al., 2018). Blood flow in the aorta possesses a significant helical component due to the complex aortic morphology (Morbidity et al., 2013) and the helicity of the flow patterns can

\* Corresponding author at: 158 cours Fauriel, 42023 Saint-Etienne cedex 2, France.

E-mail address: [avril@emse.fr](mailto:avril@emse.fr) (S. Avril).

be altered in BAV patients (Garcia et al., 2017) and in ATAA patients (Frydrychowicz et al., 2012).

CFD is an appropriate computational method to simulate blood flows in the aorta (Yu et al., 2016; Chen et al., 2017; Bakhshinejad et al., 2017; Jayendiran et al., 2020). Most of the simulation studies that have been published in the literature on this topic used idealized inlet boundary conditions rather than patient specific velocity maps (Pasta et al., 2013; Stevens et al., 2017). Hence there is a need to explore more accurately hemodynamics alterations related to TAVs and BAVs using CFD. The combination of 4D flow MRI and CFD presents a promising method to address this need (Callaghan et al., 2015; Romarowski et al., 2018).

Therefore, the main goal of this study is to characterize the effect of valve phenotype on the hemodynamics descriptors, namely time-averaged WSS and helicity, in the dilated ascending aortic region using CFD with inflow boundary conditions derived from 4D flow MRI. As hemodynamics calculations need to be accurate, a secondary goal was to verify the accuracy of the calculations by assessing the agreement between the CFD simulations and the 4D flow MRI measurements.

## 2. Methods

### 2.1. Data acquisition

4D flow MRI data-sets obtained from 3T MR scanner (Magnetom Prisma, Siemens, Erlangen) were used to assess blood flows in the ascending thoracic aorta (ATA) from 12 subjects (Table 1). The protocol was approved by the Institutional Review Board of the University Hospital Center of Saint-Etienne and an informed consent was obtained from the participants. The axial cross sectional images at predefined anatomic levels were used for measuring the ATA maximum diameter. We measured outer to outer diameter knowing that there is no convention about measuring the luminal or outer to outer diameter of the aorta (Boehm et al., 2015). The discussion regarding the patient characteristics are given in Section B in the supplementary materials.

All the patients were assessed for the presence of functional valvular defects by standard transthoracic echocardiography. The echocardiographic exam relies on three parameters, namely the peak velocity, the mean pressure gradient and the aortic valve area. The first two parameters are directly calculated from Doppler, whereas the aortic valve area is derived from measurement of the left ventricular outflow tract (LVOT) diameter, LVOT time-velocity integral (TVI) and aortic TVI using the continuity equation.

### 2.2. Numerical simulation

The reconstructed patient-specific geometry from 4D flow MRI data, including the ATA starting from sinotubular junction (STJ),

aortic arch with branches (brachiocephalic artery (BCA), left common carotid artery (LCC) & left subclavian artery (LSUB)) and the descending aorta, was imported in Ansys Fluent (ANSYS, Academic research, Release 17.2) and meshed with tetrahedral cells for further analysis. Details regarding the methodology are given in Section A in the supplementary materials.

### 2.3. Estimation of flow parameters

The flow eccentricity was calculated as follows (Condemi et al., 2019),

$$Flow_{eccentricity} = \frac{\sqrt{\sum_j (C_j - C_j^{vel})^2}}{D} \quad j = x, y, z; \quad (1)$$

Where  $C_j$ ,  $C_j^{vel}$  and  $D$  are the coordinates of the lumen center (Fig. S1 in the supplementary materials), center of velocity and diameter, respectively.

The center of velocity  $C_j^{vel}$  was calculated as the average position of lumen pixels ( $r_{ij}$ ), weighted by the velocity information ( $v_i$ ) as given in Eq. 2 (Sigovan et al., 2011)

$$C_j^{vel} = \frac{\sum_i r_{ij} |v_i|}{\sum_i |v_i|} \quad i = \text{lumen pixels } (x, y, z), \quad j = x, y, z; \quad (2)$$

Flow eccentricity equal to 0 indicates that the flow is centrally distributed along the length of the vessel and 1 indicates that the flow is fully eccentric.

The local normalized helicity (LNH) corresponds to the local value of the cosine of the angle between the velocity  $V$  and vorticity  $\omega$  (Garcia et al., 2017)

$$LNH = \frac{V \cdot \omega}{|V||\omega|} \quad (3)$$

LNH varies between  $-1$  (left-handed rotation) and  $1$  (right-handed rotation) with  $0$  indicating a symmetrical flow (Manuel et al., 2009; Condemi et al., 2017). An optimal LNH threshold detecting differences between patients and the healthy group is set as  $0.6$  based on the study conducted by Garcia et al. (2017). At each threshold the percentage of the total volume occupied by the isosurface volume was assessed. For example, the % volume of absolute  $LNH \geq 0.6$  was calculated from the iso-surface volume (% volume of absolute  $LNH \geq 0.6 = \text{volume of absolute } LNH \geq 0.6 / \text{Total volume} \times 100$ ).

The TAWSS value was calculated such as (Condemi et al., 2019),

$$TAWSS = \frac{1}{T} \int_0^T WSS(t) dt \quad (4)$$

**Table 1**

Test of significance for TAV ATAA versus BAV ATAA patient characteristics and hemodynamics descriptors.

	Parameters	TAV ATAA	BAV ATAA	Sig (2-tailed) TAV ATAA vs BAV ATAA
Patient characteristics	Age, Years	59.60 ± 11.63	58.20 ± 5.59	0.817
	Weight, kg	75.40 ± 18.63	73.20 ± 11.38	0.829
	Height, m	1.67 ± 0.13	1.66 ± 0.03	0.779
	BSA	1.85 ± 0.26	1.83 ± 0.14	0.855
	Maximum ATAA diameter, mm	43.94 ± 3.66	45.55 ± 1.14	0.393
	Inlet angle, $\theta$	33.65 ± 3.84	32.59 ± 5.21	0.725
Hemodynamics parameters	Flow eccentricity at Section 1'	0.39 ± 0.05	0.43 ± 0.01	0.268
	Flow eccentricity at Section 2'	0.82 ± 0.11	0.85 ± 0.03	0.575
	% Surface area with TAWSS $\geq 3$ Pa	0.33 ± 0.49	3.08 ± 4.05	0.282
	% Surface area with TAWSS $\leq 1$ Pa	78.96 ± 14.19	85.28 ± 12.95	0.483
	% Volume with absolute LNH $\geq 0.6$	2.02 ± 1.96	1.11 ± 0.53	0.367
	% Volume with absolute LNH $\leq 0.4$	88.50 ± 6.72	93.38 ± 5.21	0.235

where  $T$  is the period of the cardiac cycle and  $WSS$  is the instantaneous wall shear stress. The % surface area with  $TAWSS \leq 1$  Pa was derived, being defined as the surface area with  $TAWSS \leq 1$  Pa/Total surface area  $\times 100$ .

#### 2.4. Statistical analyses

The statistical analysis was performed with SPSS 17 (IBM SPSS software, Chicago). A Bland Altman analysis was performed to evaluate the agreement between the CFD simulation and the 4D flow MRI measured flow eccentricity. A 2-tailed independent samples t-test was conducted to evaluate the significant differences between TAV and BAV ATAA. The deduced parameters namely flow eccentricity, TAWSS and absolute LNH in the ATA between TAV and BAV were compared using an independent-sample t-test. A pre-determined level of significance equal to 95% and p-values  $< 0.05$  were considered as significant.

### 3. Results

#### 3.1. Comparison between CFD-calculated and 4D flow MRI-measured velocities and flows

In order to ensure that the velocity profiles obtained from 4D flow MRI at different time frames throughout the cardiac cycle are correctly estimated by CFD, we have compared the time-averaged velocity profiles from CFD simulations with the 4D flow MRI. Agreement between the 4D flow MRI and CFD profiles should be satisfied as the former was used to assign boundary conditions of the latter. However, interpolation was required to assign the boundary conditions at the correct times as time steps of the CFD analysis did not coincide with the times at which the MRI data were acquired. The time-averaged velocity profiles obtained from 4D flow MRI and CFD are shown in Fig. 1.

Flow eccentricity calculated near the dilated region (Section 2' with largest diameter in the dilated region shown in Fig. S2) from 4D flow MRI during the systolic phase was compared with the CFD simulations using Bland-Altman plot. The estimated bias was  $-0.01085$ , standard deviation of bias was  $0.0353$ , the 95% limits of agreement varied from  $-0.080$  (blue dotted line) to  $0.058$  (red dashed line) and the continuous brown line represents the mean (Fig. 2). All data points remained in the 95% limit band (average difference  $\pm 1.96$  standard deviation of the difference), indicating the good agreement between the 4D flow MRI measurements and the CFD simulation quantitatively.

#### 3.2. Streamlines

The streamlines obtained from the simulations at peak systole for different cases are shown in Fig. 3. The streamline contours for both BAV and TAV ATAA patients showed that the flow starts detaching from the aortic wall and a vortex is formed near the dilated ATA region. In healthy subjects the flow is found to be laminar and evenly distributed through the cross-section of the aorta near the ATA region.

#### 3.3. TAWSS

TAWSS was obtained for TAV ATAA, BAV ATAA and healthy subjects (Figs. 4–6). Both TAV ATAA and BAV ATAA patients exhibited low TAWSS (i.e.  $\leq 1$  Pa) in the ATA region. The surface area of the ATA with  $TAWSS \geq 3$  Pa and  $\leq 1$  Pa were evaluated (Table 2). Irrespectively of the valve phenotype, all patients, except patient 4, have large surface area (i.e. varying between 70% and 99%) with low TAWSS (i.e.  $\leq 1$  Pa). High TAWSS (i.e.  $\geq 3$  Pa) were found only

in small regions ( $\leq 1\%$  surface area) of the ATA in 8 out of 10 patients, whereas patient 6 and 8 have 8% and 7% of the surface area with  $TAWSS \geq 3$  Pa. Healthy subjects have surface area  $\geq 25\%$  with high TAWSS ( $\geq 3$  Pa) and  $\approx 20\%$  surface area with low TAWSS ( $\leq 1$  Pa).

#### 3.4. Helicity

The LNH magnitude was extracted for all patients and healthy subjects (Figs. 4, 5, & 6). It was observed that large absolute LNH values were more prominent in ATAA patients than healthy subjects. In ATAA patients the % volume with absolute LNH  $\geq 0.6$  is  $> 2$  and absolute LNH  $\leq 0.4$  varies between 80 and 95. In healthy subjects, more than 98% volume has an absolute LNH below 0.4 and less than 1% volume has absolute LNH  $\geq 0.6$  (Table 2).

#### 3.5. Correlation between flow eccentricity and hemodynamics descriptors

A significant correlation is obtained between flow eccentricity at Section 2' = ascending aortic region with maximum diameter and flow eccentricity at Section 1' = sinotubular junction - also referred as aortic inlet in this paper. Hence, we also studied correlation between flow eccentricity at Section 2' and WSS, TAWSS and LNH biomarkers. Fig. 7 summarizes the independent associations between parameters such as flow eccentricity at Section 1', % surface area with  $TAWSS \leq 1$  Pa, % volume with absolute LNH  $\geq 0.6$ , maximal ATAA diameter and inlet angle with flow eccentricity at Section 2'. Strong and significant correlations exist between flow eccentricity at Section 1' ( $R^2 = 0.655$ ,  $p = 0.040$ ), % surface area with  $TAWSS \leq 1$  Pa ( $R^2 = 0.697$ ,  $p = 0.025$ ), % volume with absolute LNH  $\geq 0.6$  ( $R^2 = 0.964$ ,  $P < 0.001$ ), maximal ATAA diameter ( $R^2 = 0.664$ ,  $p = 0.036$ ) with flow eccentricity at Section 2'. But there is no significant correlation between the inlet angle ( $R^2 = 0.261$ ,  $p = 0.467$ ) and the flow eccentricity at Section 2'.

#### 3.6. Correlation between maximum ATAA diameter and hemodynamics descriptors

A significant correlation was found between the diameter and hemodynamics descriptors namely TAWSS and helicity (Fig. 8). For instance, regarding the % of surface area with  $TAWSS \leq 1$  Pa significance is valued at  $R^2 = 0.688$ ,  $p = 0.028$  and for the % of volume with absolute LNH  $\geq 0.6$  significance is valued at  $R^2 = 0.650$ ,  $p = 0.045$ . The increase in maximal ATAA diameter affects the hemodynamics descriptors for both TAV ATAA and BAV ATAA patients.

#### 3.7. Significance of differences in hemodynamics descriptors between TAV and BAV ATAA patients

Hemodynamics descriptors, namely flow eccentricity, TAWSS and helicity in TAV and BAV groups were compared using 2-tailed independent samples t-test. Results are reported in Table 1. The data are presented as mean  $\pm$  standard deviation (max, min). The parameters such as flow eccentricity at Section 1' ( $p = 0.268$ ), flow eccentricity at Section 2' ( $p = 0.575$ ), % surface area with  $TAWSS \geq 3$  Pa ( $p = 0.282$ ), % surface area with  $TAWSS \leq 1$  Pa ( $p = 0.483$ ), % volume with absolute LNH  $\geq 0.6$  ( $p = 0.367$ ) and % volume with absolute LNH  $\leq 0.4$  ( $p = 0.235$ ) have a p-value  $> 0.05$ . The significance  $> 0.05$  shows that the hemodynamics descriptors obtained from TAV and BAV patient were not significantly different.

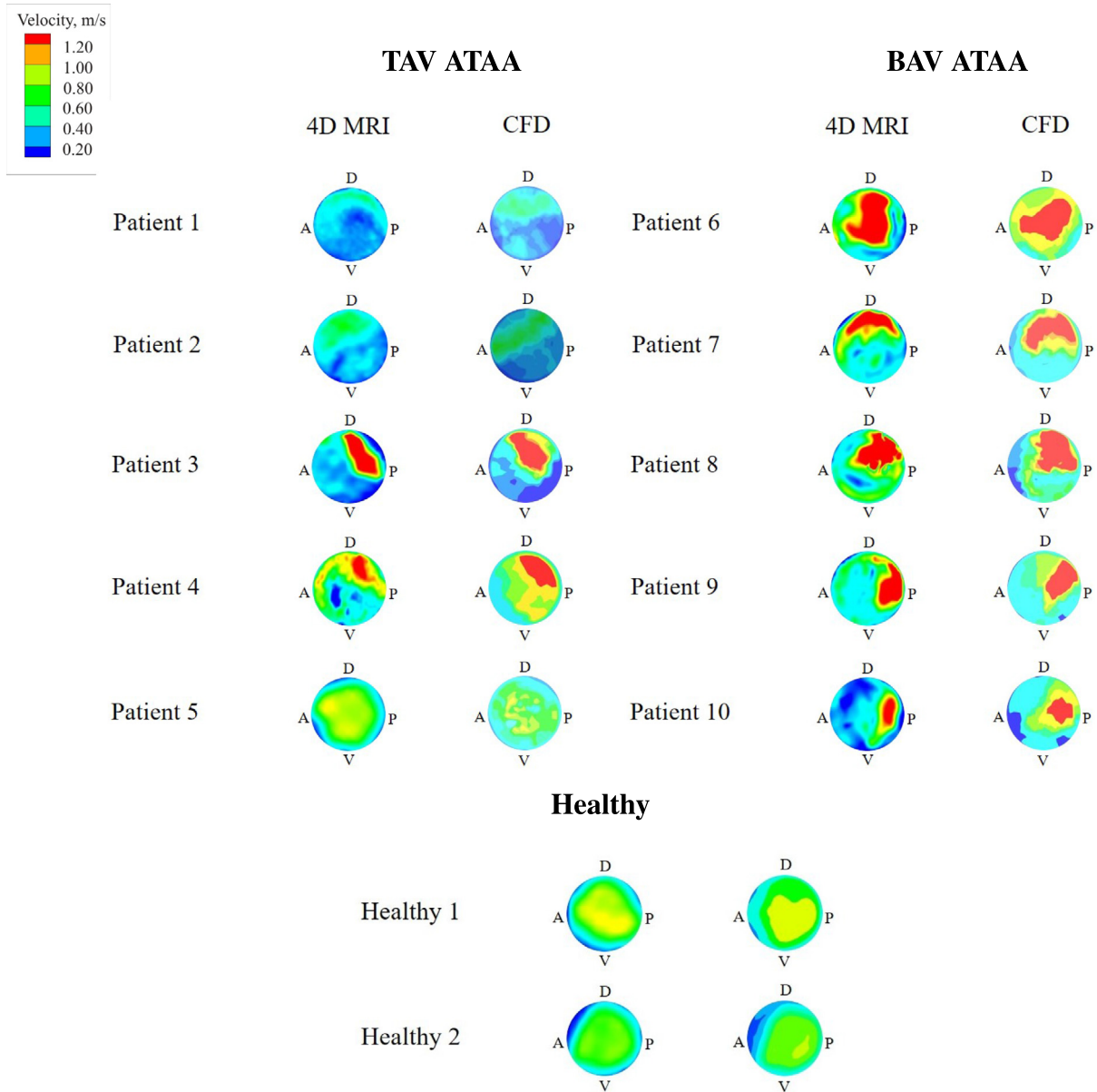


**Fig. 1.** Time-averaged velocity profiles obtained from 4D flow MRI and CFD at the inlet. The dorsal (D), ventral (V), anterior (A) and posterior (P) regions are defined according to Fig. S1 in the supplementary materials.

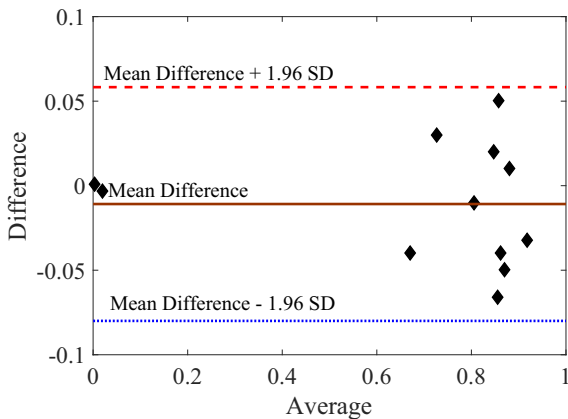


**Fig. 2.** Bland-Altman plot showing 4D flow MRI vs CFD  $Flow_{eccentricity}$  obtained from time-averaged velocity profiles near the ATA region.

**4. Discussion**

This study showed that flow eccentricity at the aortic root is a major determinant of hemodynamics alterations in ATAAs, such as low TAWSS and elevated absolute LNH values are independent of the aortic valve phenotype. The flow eccentricity at the aortic root indicates a dysfunction of the aortic valve and is frequent with BAV phenotype. But the relation between eccentricity downstream and WSS, TAWSS & LNH biomarkers remains to be elucidated, especially how the enlargement of aortic diameter in aneurysms participates to increase the flow disturbance caused by eccentricity at the aortic root.

Our CFD simulations are time resolved and provide estimations of the velocity maps at different timeframes. Only after running the simulations, at the post-processing stage, we eventually compute time-averaged metrics to compare the groups of subjects. The time-averaged velocities obtained from CFD analyses were vali-

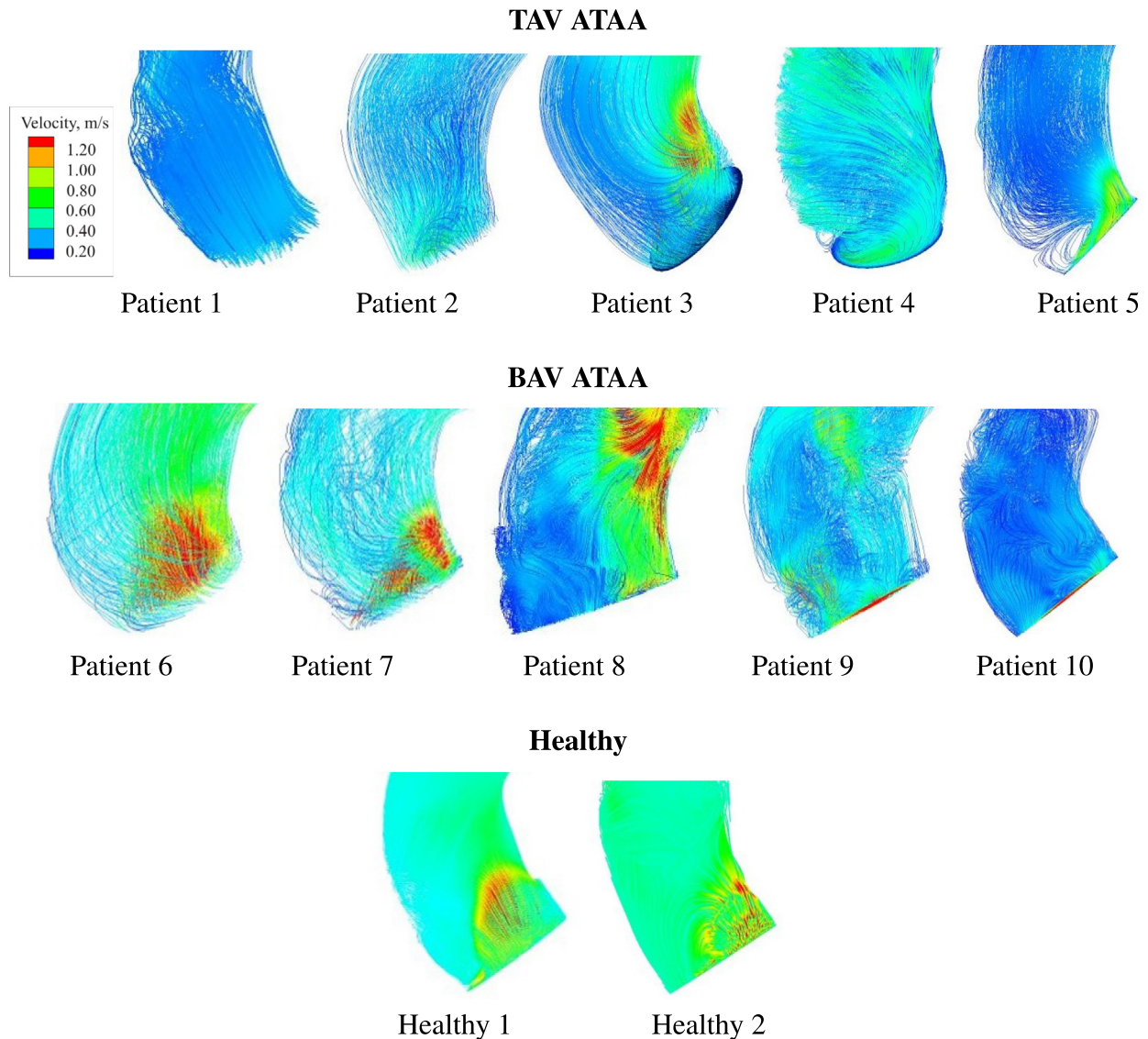


**Fig. 3.** Streamlines of blood velocity at peak systole for TAV ATAA, BAV ATAA and healthy subjects.

dated against MRI data justifying the significance of time-averaged metrics derived from CFD analyses.

Among studies related to BAV and TAV patients, [Hope et al. \(2011\)](#) and [Pasta et al. \(2013\)](#) compared the blood flow patterns between TAV and BAV in patients harbouring ATAA. One of the two was based on 4D flow MRI to measure *in vivo* 3D blood flow velocities in the aorta, finding abnormal eccentric flow and asymmetric WSS for both BAV and TAV patients ([Hope et al., 2011](#)). The other study was based on CFD simulations, showing a slight difference in the helical flow patterns between TAV and BAV ATAA patients ([Pasta et al., 2013](#)) but they did not consider patient specific velocity patterns. Our study proposed a framework combining 4D flow MRI and CFD to compute ATAA hemodynamics.

We found that blood flow disturbance near the dilated region generates vortices in TAV and BAV ATAAs and not in the healthy subjects ([Weingang et al., 2008](#); [Sigovan et al., 2011](#); [Pasta et al., 2013](#); [Numata et al., 2016](#)). The flow disturbance refers here to the existence of retrograde flows and recirculation areas ([Chiu and Chien, 2011](#)). The vortices manifest with flow eccentricity and non-uniform distribution of WSS, potentially causing accumulation of atherogenic particles at the endothelial surface ([Deng et al., 2008](#); [Ethier, 2002](#); [Tarbell, 2003](#); [Chiu and Chien, 2011](#)).

As we assumed rigid and impermeable walls ([Torii et al., 2009](#); [Steinman, 2012](#)), we focused our analysis on TAWSS values only, not on temporal variations of WSS. TAWSS contours of both TAV and BAV ATAAs show large areas with TAWSS lower than 1 Pa. In healthy subjects the area fraction occupied by TAWSS  $\leq 1$  Pa and  $\geq 3$  Pa was significantly lower. The increase in flow eccentricity near the dilated region induces a decrease of the TAWSS magnitude. More surface is occupied by low TAWSS in TAV and BAV ATAAs. Commonly TAWSS in healthy arteries is between 1 and 7 Pa ([Nordgaard et al., 2010](#)). Low TAWSS (i.e.  $\leq 1$  Pa) in a large area fraction of the aortic vessel indicates possible endothelial dysfunction and progress in vascular disease ([Nordgaard et al., 2010](#); [Papadopoulos et al., 2016](#); [Numata et al., 2016](#)). If the TAWSS is larger than 7 Pa, endothelial damage can also be induced but the mechanisms of this damage have not yet been fully elucidated ([Fukumoto et al., 2008](#)). TAWSS also shows good correlation with maximal ATAA diameter. With increased ATAA diameter, the percentage of area with low TAWSS increases.

LNH contours show that both TAV ATAA and BAV ATAA have large volumes with elevated absolute LNH (i.e.  $\geq 0.6$ ) compared to healthy subjects. These results are in agreement with previous studies where elevated helicity was found in ATAA patients

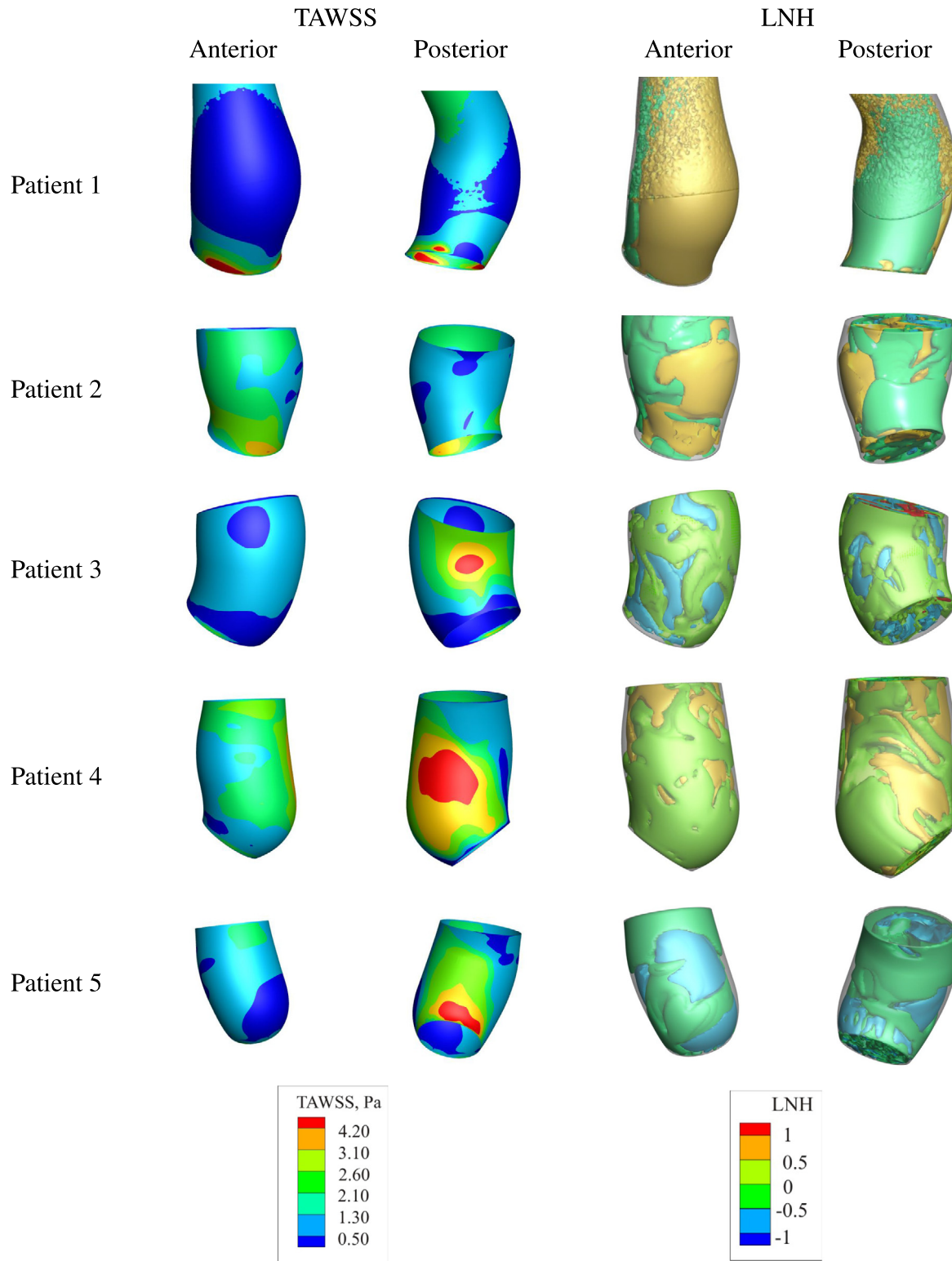


Fig. 4. TAWSS and LNH distribution in the ATA region for TAV ATAA patients.

(Lorenz et al., 2014; Garcia et al., 2017). It was observed that the % volume of absolute LNH  $\geq 0.6$  had a significant correlation with flow eccentricity and maximal ATAA diameter. Eventhough there are many studies indicating the role of helicity in the development of cardiovascular diseases (Kilner et al., 1993; Caro et al., 1996; Stonebridge et al., 1996; Morbiducci et al., 2007; Liu et al., 2009; Liu et al., 2014), it is yet unclear how these hemodynamics alter-

ations affect wall remodeling in ATAAs (Gataulin et al., 2015; Ha et al., 2016).

The correlation analysis between the aortic valve phenotype and the hemodynamics descriptors shows that TAV and BAV ATAA patients have no significant difference in terms of blood flow patterns and hemodynamics descriptors (refer Table 1). Patients with both aortic valve phenotypes have shown more region with low

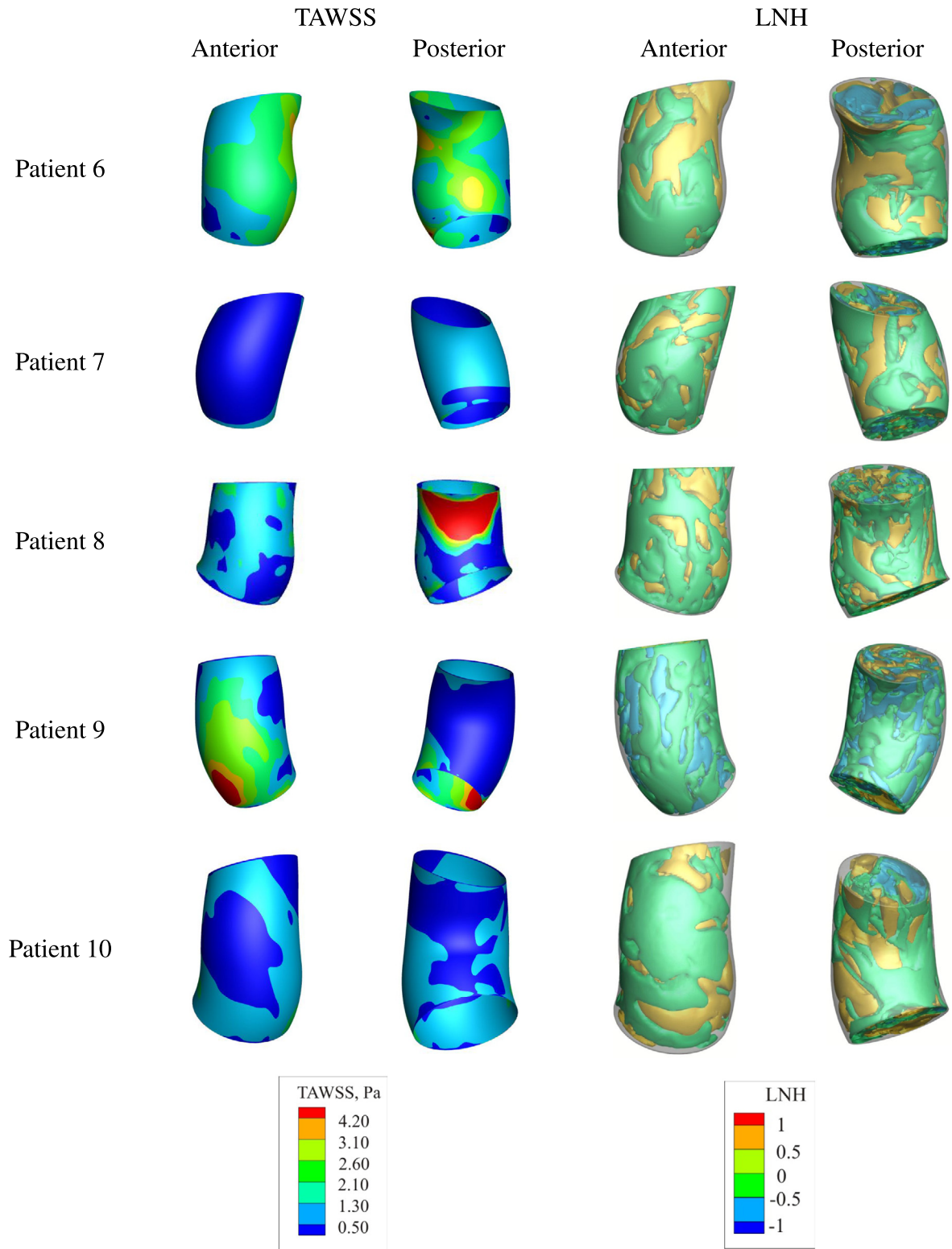


Fig. 5. TAWSS and LNH distribution in the ATA region for BAV ATAA patients.

TAWSS, elevated absolute LNH and pronounced flow eccentricity near the dilated ATA region. Irrespective of the aortic valve phenotype the alteration in hemodynamics parameters was due to flow eccentricity patterns.

Basically the aortic valve condition should be classified based on:

- (1) the morphological condition (phenotype) which relates to the natural feature of the valve (BAV or TAV)
- (2) the functional condition which relates to the behaviour of the valve during the cardiac cycle. It can be quantified in terms of hemodynamics descriptor, namely the flow eccentricity

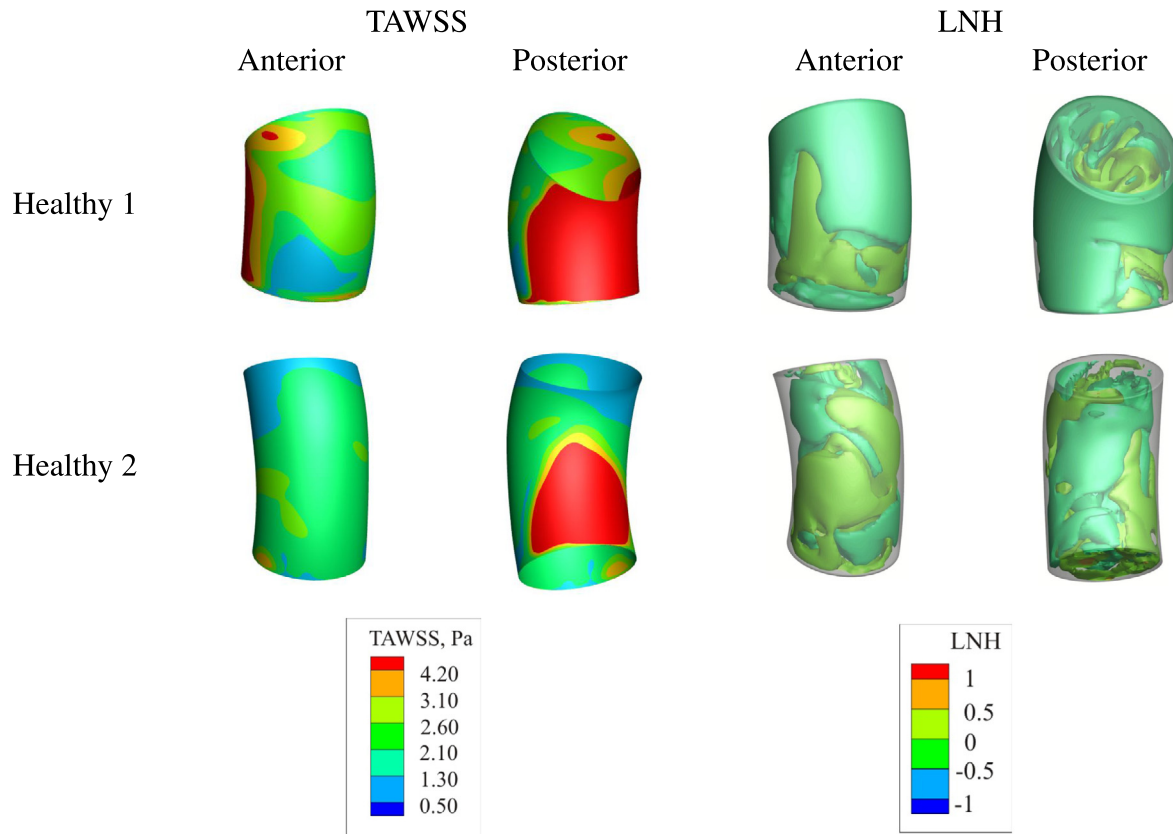


Fig. 6. TAWSS and LNH distribution in the ATA region for healthy subjects.

**Table 2**  
Percentage of TAWSS area and absolute LNH volume for TAV ATAA, BAV ATAA patients and healthy subjects.

		% surface area with TAWSS		% volume with absolute LNH	
		$\geq 3$ Pa	$\leq 1$ Pa	$\geq 0.6$	$\leq 0.4$
TAV ATAA	Patient 1	0.10	98.7	2.10	90.4
	Patient 2	0.12	76.8	2.60	89.4
	Patient 3	0.10	83.4	2.10	91.5
	Patient 4	1.20	59.3	3.10	80.9
	Patient 5	0.15	76.6	5.50	82.3
BAV ATAA	Patient 6	8.00	71.0	3.10	85.0
	Patient 7	0.15	99.7	2.40	91.9
	Patient 8	7.00	80.0	2.10	93.8
	Patient 9	0.15	77.4	2.80	94.2
	Patient 10	0.10	98.3	2.10	93.2
Healthy	Healthy 1	28.5	20.5	0.50	98.6
	Healthy 2	27.3	20.1	0.40	98.7

In the present work we have shown that both BAV and TAV can have similar functional conditions. This may explain why it is very difficult to establish correlations between the valve phenotype and the aneurysm rupture risk (Agnese et al., 2019; Forsell et al., 2014; Kjellqvist et al., 2013; Ikonomidis et al., 2007; Corte et al., 2008).

In our 5 BAV patients, only two of them presented a mild degree of AR, the rest had BAV phenotypes without any gradient or AR degree. Accordingly, the functional status of the aortic valve seems to influence the ATA flow patterns. This was also previously demonstrated for AS, with good correlations between the AS degree and ATAA flow patterns (Frag et al., 2018). Moreover, almost 50% of BAV patients never develop ATAA and keep normal functions during the entire lifetime without treatment (Pedersen et al., 2019). Reciprocally, diseased tri-leaflet aortic valves can acquire abnormal opening just like bi-leaflet valves inducing

eccentric flows at the aortic root. Therefore, the aortic valve functional condition (characterized by flow eccentricity at the aortic root) rather than the phenotype is a major factor in determining hemodynamics alterations in the ATA (Fig. 3).

There are some limitations in this study. The sample size was limited to 10 patients and 2 healthy subjects. Ooij et al. (2017) found significant differences in peak systolic WSS between a large group of BAV ( $n = 136$ ) and TAV ( $n = 213$ ) with no AS. In the present study we could not find any differences between TAWSS in BAV and TAV. It may be due to the small sample size and/or the fact that averaging out WSS patterns over time does not reveal differences.

CFD simulations were based on the assumption of rigid and impermeable walls. The comparison between the CFD and 4D flow MRI time-averaged velocity maps shows some differences in some patients. This may be induced by the interpolation effects, but also

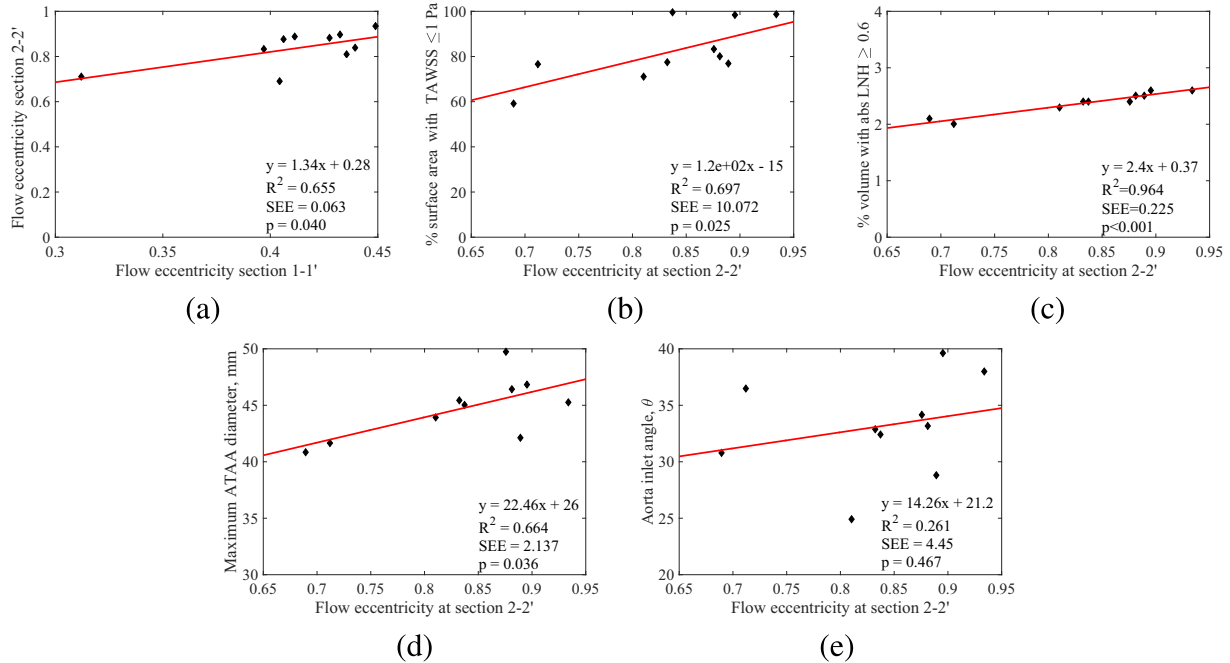


Fig. 7. Correlation between the flow eccentricity near the dilated region and other significant parameters (hemodynamics and morphology).

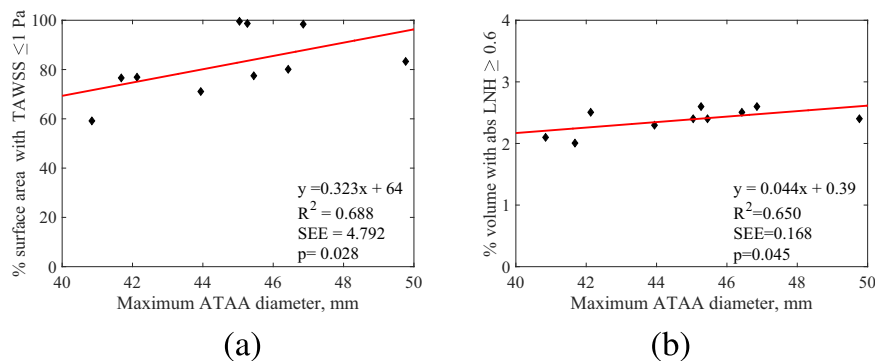


Fig. 8. Correlation between the maximum ATAA diameter and hemodynamic parameters.

due to outlet boundary conditions and the rigid wall assumption. These assumptions are usually reasonable for flow and WSS predictions in finite segments of large arteries (Steinman, 2012) although they may induce errors in evaluating temporal variations of WSS. The velocity distribution obtained from 4D flow MRI was used as inlet boundary condition for the simulation. As 4D flow MRI datasets are noisy, this can be transmitted to the computational predictions. However these datasets permit to assign patient-specific boundary conditions to the model, which is essential for modelling hemodynamics computationally.

## 5. Conclusions

This study demonstrated that the flow eccentricity at the aortic root influences the blood flow patterns in ATAA patients independently of the aortic valve phenotype. Flow eccentricity values across the dilated region have significant correlation with TAWSS, absolute LNH and maximal ATAA diameter, however they have no correlation with the inlet angle. Knowing the crit-

ical role of flow eccentricity in hemodynamics alterations, it will be important to determine how it interacts with other critical factors of ATAA such as aortic wall remodeling and smooth muscle cell differentiation.

## Declaration of Competing Interest

There is no conflict of interest.

## Acknowledgments

This research work was supported by the European Research Council (ERC grant biolochanics, Grant No. 647067). We are also grateful to Ansys, Inc. for providing Ansys Fluent (ANSYS® Academic Research, Release 17.2). The authors thank Siemens Healthineers for their technical support and more specifically Ning Jin, Andreas Greiser and Sinyeob Ahn for making available the 4D flow 785A prototype sequence.

## Appendix A. Supplementary material

Supplementary data associated with this article can be found, in the online version, at <https://doi.org/10.1016/j.jbiomech.2020.109954>.

## References

- Agnese, V., Pasta, S., Michelena, H.I., Mina, C., Romano, G.M., Carerj, S., Zito, C., Maalouf, J.F., Foley, T.A., Raffa, G., Clemenza, F., Pilato, M., Bellavia, D., 2019. Patterns of ascending aortic dilatation and predictors of surgical replacement of the aorta: A comparison of bicuspid and tricuspid aortic valve patients over eight years of follow-up. *J. Mol. Cell. Cardiol.* 135, 31–39.
- Azadani, A.N., Chitsaz, S., Mannion, A., Mookhoek, A., Wisneski, A., Guccione, J.M., Hope, M.D., Ge, L., Tseng, E.E., 2013. Biomechanical Properties of Human Ascending Thoracic Aortic Aneurysms. *Ann. Thorac. Surg.* 9, 50–58.
- Baeyens, N., Bandyopadhyay, C., Coon, B.G., Yun, S., Schwartz, M.A., 2016. Endothelial fluid shear stress sensing in vascular health and disease. *J. Clin. Invest.* 126, 821–828.
- Bakhshinejad, A., Baghaie, A., Vali, A., Saloner, D., Rayz, V.L., D'Souza, R.M., 2017. Merging computational fluid dynamics and 4d flow mri using proper orthogonal decomposition and ridge regression. *J. Biomech.* 58, 162–173.
- Barker, A.J., Lanning, C., Shandas, R., 2010. Quantification of hemodynamic wall shear stress in patients with bicuspid aortic valve using phase-contrast MRI. *Ann. Biomed. Eng.* 38, 788–800.
- Barker, A.J., Markl, M., Burk, J., Lorenz, R., Bock, J., Bauer, S., Schulz-Menger, J., Brenkenhoff, F.V.K., 2012. Bicuspid Aortic Valve Is Associated With Altered Wall Shear Stress in the Ascending Aorta. *Circ. Cardiovasc. Imag.* 5, 457–466.
- Biglino, G., Cosentino, D., Steeden, J.A., Nova, L.D., Castelli, M., Ntsinjana, H., Pennati, G., Taylor, A.M., Schievano, S., 2015. Using 4D Cardiovascular Magnetic Resonance Imaging to Validate Computational Fluid Dynamics: A Case Study. *Front. Pediatr.* 3, 1–10.
- Bissell, M.M., Hess, A.T., Biasioli, L., Glaze, S.J., Loudon, M., Pitcher, A., Davis, A., Prendergast, B., Markl, M., Barker, A.J., Neubauer, S., Myerson, S.G., 2013. Aortic Dilation in Bicuspid Aortic Valve Disease. *Circ. Cardiovasc. Imag.* 6, 499–507.
- Boehm, N.K., Maceira, A., Buechel, E.R.V., Claussen, J.V., Turkbey, E.B., Williams, R., Plain, S., Tee, M., Eng, J., Bluemke, D.A., 2015. Normal values for cardiovascular magnetic resonance in adults and children. *J. Cardiovasc. Magn. Reson.*, 17–29.
- Callaghan, F.M., Karkouri, J., Broadhouse, K., Evin, M., Fletcher, D.F., Grieve, S.M., 2015. Thoracic aortic aneurysm: 4D flow MRI and computational fluid dynamics model. *Comput. Methods Biomech. Biomed. Eng.* 18, 1894–1895.
- Caro, C.G., Doory, D.J., Tarnawski, M., Scott, K.T., Long, Q., Dumoulin, C.L., 1996. Non-planar curvature and branching of arteries and non-planar-type flow. *Proc. Roy. Soc. A* 452, 185–197.
- Chen, Z., Yu, H., Shi, Y., Zhu, M., Wang, Y., Hu, X., Zhang, Y., Chang, Y., Xu, M., Gao, W., 2017. Vascular Remodelling Relates to an Elevated Oscillatory Shear Index and Relative Residence Time in Spontaneously Hypertensive rats. *Scient. Rep.* 7, 1–10.
- Chiu, J.J., Chien, S., 2011. Effects of Disturbed Flow on Vascular Endothelium: Pathophysiological Basis and Clinical Perspectives. *Phys. Rev.* 91, 327–387.
- Condemi, F., Campisi, S., Viallon, M., Croisille, P., Avril, S., 2019. Relationship between ascending thoracic aortic aneurysms hemodynamics and biomechanical properties. *IEEE Trans. Biomed. Eng.* <https://doi.org/10.1109/TMI.2019.2924955>.
- Condemi, F., Campisi, S., Viallon, M., Troalen, T., Xuexin, G., Barker, A.J., Markl, M., Croisille, P., Trabelsi, O., Cavinato, C., Duprey, A., Avril, S., 2017. Fluid- and Biomechanical Analysis of Ascending Thoracic Aorta Aneurysm with Concomitant Aortic Insufficiency. *Ann. Biomed. Eng.* 45, 2921–2932.
- Corte, A.D., Quarto, C., Bancone, C., Castaldo, C., Meglio, F.D., Nurzynska, D., Santo, L. S.D., Feo, M.D., Scardone, M., Montagnani, S., Cotrufo, M., 2008. Spatiotemporal patterns of smooth muscle cell changes in ascending aortic dilatation with bicuspid and tricuspid aortic valve stenosis: Focus on cell-matrix signaling. *J. Thorac. Cardiovasc. Surg.* 135, 8–18.
- Deng, X., Marois, Y., How, T., Merhi, Y., King, M., Guidoin, R., Karino, T., 2008. Luminal surface concentration of lipoprotein (LDL) and its effect on the wall uptake of cholesterol by canine carotid arteries. *J. Vasc. Surg.* 21, 135–145.
- Ethier, C.R., 2002. Computational modeling of mass transfer and links to atherosclerosis. *Ann. Biomed. Eng.* 30, 461–471.
- Farag, E.S., Ooij, P.V., Planken, R.N., Dukker, K.C.P., de Heer, F., Bouma, B.J., Visser, D. R., Groenink, M., Nederveen, A.J., de Mol, B.A.J.M., Kluijn, J., Boekholdt, S.M., 2018. Aortic valve stenosis and aortic diameters determine the extent of increased wall shear stress in bicuspid aortic valve disease. *J. Mag. Res. Imag.* 48, 522–530.
- Farzaneh, S., Trabelsi, O., Avril, S., 2018. Inverse identification of local stiffness across ascending thoracic aortic aneurysms. *Biomechan. Model. Mechanobiol.* <https://doi.org/10.1007/s10237-018-1073-0>.
- Forsell, C., Björck, H.M., Eriksson, P., Cereceda, A.F., Gasser, T.C., 2014. Biomechanical Properties of the Thoracic Aneurysmal Wall: Differences Between Bicuspid Aortic Valve and Tricuspid Aortic Valve Patients. *Ann. Thorac. Surg.* 98, 65–71.
- Frydrychowicz, A., Berger, A., Rio, A.M.D., Russe, M.F., Bock, J., Harloff, A., Markl, M., 2012. Interdependencies of aortic arch secondary flow patterns, geometry, and age analysed by 4-dimensional phase contrast magnetic resonance imaging at 3 tesla. *Euro. Radiol.* 22, 1122–1130.
- Fukumoto, Y., Hiro, T., Fujii, T., Hashimoto, G., Fujimura, T., Yamada, J., Okamura, T., Matsuzaki, M., 2008. Localized Elevation of Shear Stress Is Related to Coronary Plaque Rupture: A 3-Dimensional Intravascular Ultrasound Study With In-Vivo Color Mapping of Shear Stress Distribution. *J. Amer. Coll. Cardio.* 51, 645–650.
- García, J., Barker, A.J., Collins, J.D., Carr, J.C., Markl, M., 2017. Volumetric quantification of absolute local normalized helicity in patients with bicuspid aortic valve and aortic dilatation. *Magn. Reson. Med.* 78, 689–701.
- Gataulin, Y.A., Zaitsev, D.K., Smirnov, E.M., Fedorova, E.A., Yuhnev, A.D., 2015. Weakly swirling flow in a model of blood vessel with stenosis: Numerical and experimental study. *St. Petersburg Polytechnical Univ. J.: Phys. Math.* 1, 364–371.
- Girdauskas, E., Borger, M.A., Secknus, M.A., Girdauskas, G., Kuntze, T., 2011. Is aortopathy in bicuspid aortic valve disease a congenital defect or a result of abnormal hemodynamics? A critical reappraisal of a one-sided argument. *Euro. J. Cardio. Thorac. Surg.* 39, 809–814.
- Guzzardi, D.G., Baker, A.J., Ooij, P.V., Malaisrie, S.C., Putjmana, J.J., Belke, D.D., Mewhort, H.E.M., Svystonyuk, D.A., Kang, S., Verma, S., Collins, J., Carr, J., Bonow, R.O., Markl, M., Thomas, J.D., McCarthy, P.M., Fedak, P.W.M., 2015. Valve-Related Hemodynamics Mediate Human Bicuspid Aortopathy. *J. Amer. Coll. Cardio.* 66, 892–900.
- Ha, H., Kim, G.B., Kweon, J., Lee, S.J., Kim, Y.H., Kim, N., Yang, D.H., 2016. The influence of the aortic valve angle on the hemodynamic features of the thoracic aorta. *Scient. Reports* 6, 1–14.
- Hope, M.D., Hope, T.A., Crook, S.E., Ordovas, K.G., Urbani, T.H., Alley, M.T., Higgins, C.B., 2011. 4D flow CMR in assessment of valve-related ascending aortic disease. *J. Amer. Coll. Cardio.: Cardiovascular Imag.* 4, 781–787.
- Ikonomidis, J.S., Jones, J.A., Barbour, J.R., Stroud, R.E., Clark, L.L., Kaplan, B.S., Zeeshan, A., Bavaria, J.E., Gorman, J.H., Spinale, F.G., Gorman, R.C., 2007. Expression of matrix metalloproteinases and endogenous inhibitors within ascending aortic aneurysms of patients with bicuspid or tricuspid aortic valves. *J. Thorac. Cardiovasc. Surg.* 133, 1028–1036.
- Jayendiran, R., Condemi, F., Campisi, S., Viallon, M., Croisille, P., Avril, S., 2020. Computational prediction of hemodynamical and biomechanical alterations induced by aneurysm dilatation in patient-specific ascending thoracic aortas. *Int. J. Numer. Methods. Biomed. Eng.* <https://doi.org/10.1002/cnm.3326>.
- Kilner, P.J., Yang, G.Z., Mohiaddin, R.H., Firmin, D.N., Longmore, D.B., 1993. Helical and retrograde secondary flow patterns in the aortic arch studied by three-directional magnetic resonance velocity mapping. *Circulation* 88, 2235–2247.
- Kjellqvist, S., Maleki, S., Olsson, T., Chwastyniak, M., Branca, R.M.M., Lehtio, J., Pinet, F., Cereceda, A.F., Eriksson, P., 2013. A combined proteomic and transcriptomic approach shows diverging molecular mechanisms in thoracic aortic aneurysm development in patients with tricuspid and bicuspid aortic valve. *Mol. Cell. Prot.* 12, 407–425.
- Kwak, B.R., Back, M., Piallat, M.L.B., Caligiuri, G., Daemen, M.J.A.P., Davies, P.F., Hofer, I.E., Holvoet, P., Jo, H., Krams, R., Lehoux, S., Monaco, C., Steffens, S., Virmani, R., Weber, C., Wentzel, J.J., Evans, P.C., 2014. Biomechanical factors in atherosclerosis: mechanisms and clinical implications. *Euro. Heart J.* 35, 3013–3020.
- Lasheras, J.C., 2007. The Biomechanics of Arterial Aneurysms. *Annu. Rev. Fluid Mech.* 39, 293–319.
- Lavall, D., Schafers, H.J., Bohm, M., Laufs, U., 2012. Aneurysms of the ascending aorta. *Deutsches Arzteblatt Int.* 109, 227–233.
- Liu, X., Pu, F., Fan, Y., Deng, X., Li, D., Li, S., 2009. A numerical study on the flow of blood and the transport of LDL in the human aorta: the physiological significance of the helical flow in the aortic arch. *Amer. J. Phys. Heart. Cir. Phys.* 297, H163–H170.
- Liu, X., Sun, A., Fan, Y., Deng, X., 2014. Physiological Significance of Helical Flow in the Arterial System and its Potential Clinical Applications. *Ann. Biomed. Eng.* 43, 3–15.
- Lorenz, R., Bock, J., Barker, A.J., 2014. 4d flow magnetic resonance imaging in bicuspid aortic valve disease demonstrates altered distribution of aortic blood flow helicity. *Magn. Reson. Med.* 71, 1542–1553. e. a.
- Manuel, J., Tavares, R.S., Jorge, R.M.N., 2009. Computational Vision and Medical Image Processing. CRC Press. ISBN 9780415570411.
- Meierhofer, C., Schneider, E.P., Lyko, C., Hutter, A., Martinoff, S., Markl, M., Hager, A., Hess, J., Stern, H., Fratz, S., 2012. Wall shear stress and flow patterns in the ascending aorta in patients with bicuspid aortic valves differ significantly from tricuspid aortic valves: a prospective study. *Eur. Heart J. - Cardiovasc. Imag.* 14 (8), 797–804.
- Morbiducci, U., Ponzini, R., Gallo, D., Bignardi, C., Rizzo, G., 2013. Inflow boundary conditions for image-based computational hemodynamics: Impact of idealized versus measured velocity profiles in the human aorta. *J. Biomech.* 46, 102–109.
- Morbiducci, U., Ponzini, R., Grigioni, M., Redaelli, A., 2007. Helical flow as fluid dynamic signature for atherogenesis in aorto coronary bypass: a numeric study. *J. Biomech.* 40, 519–534.
- Muraru, D., Bidviene, J., Cavalli, G., Cavaliere, A., Badano, L.P., 2016. Tricuspid regurgitation in a patient with ascending aorta aneurysm. *Euro. Heart J. Cardiovasc. Imag.* 17, 1435.
- Nordgaard, H., Swilens, A., Nordhaug, D., Garstad, I.K., Loo, D.V., Vitale, N., Segers, P., Haaverstad, R., 2010. Impact of competitive flow on wall shear stress in coronary surgery: computational fluid dynamics of a LIMA-LAD model. *Cardiovasc. Res.* 88, 512–519.
- Numata, S., Itatani, K., Kanda, K., Doi, K., Yamazaki, S., Morimoto, K., Manabe, K., Ikemoto, K., Yaku, H., 2016. Blood flow analysis of the aortic arch using computational fluid dynamics. *Euro. J. Cardio. Thorac. Surg.* 49, 1578–1585.
- Ooij, P.V., Markl, M., Collins, J.D., Carr, J.C., Rigby, C., Bonow, R.O., Malaisrie, S.C., McCarthy, P.M., Fedak, P.W.M., Barker, A.J., 2017. Aortic valve stenosis alters expression of regional aortic wall shear stress: New insights from a 4-

- dimensional flow magnetic resonance imaging study of 571 subjects. *J. Amer. Heart Assoc.* 6, e005959.
- Papadopoulos, K.P., Gavaises, M., Pantos, I., Katrakis, D.G., Mitroglou, N., 2016. Derivation of flow related risk indices for stenosed left anterior descending coronary arteries with the use of computer simulations. *Med. Eng. Phys.* 38, 929–939.
- Pasta, S., Phillippi, J.A., Gleason, T.G., Vorp, D.A., 2012. Effect of aneurysm on the mechanical dissection properties of the human ascending thoracic aorta. *J. Thorac. Cardiovasc. Surg.* 143, 460–467.
- Pasta, S., Rinaudo, A., Luca, A., Pilato, M., Scardulla, C., Gleason, T.G., Vorp, D.A., 2013. Difference in hemodynamic and wall stress of ascending thoracic aortic aneurysms with bicuspid and tricuspid aortic valve. *J. Biomech.* 46, 1729–1738.
- Pedersen, M.W., Groth, K.A., Mortensen, K.H., Brodersen, J., Gravholt, C.H., Andersen, N.H., 2019. Clinical and pathophysiological aspects of bicuspid aortic valve disease. *Cardiol. Young* 29, 1–10.
- Pirola, S., Jarral, O.A., Regan, D.P.O., Asimakopulos, G., Anderson, J.R., Pepper, J.R., Athanasiou, T., Xu, X.Y., 2018. Computational study of aortic hemodynamics for patients with an abnormal aortic valve: The importance of secondary flow at the ascending aorta inlet. *APL Bioeng.* 2, 026101–1 – 026101–14.
- Real, E., Val-Bernal, J.F., Revuelta, J.M., Ponton, A., Diez, M.C., Mayorga, M., Higuera, J.M.L., Conde, O.M., 2014. Identification of vessel wall degradation in ascending thoracic aortic aneurysms with OCT. *Biomed. Opt. Ex.* 5, 1–12.
- Romarowski, R.M., Lefieux, A., Morganti, S., Veneziani, A., Auricchio, F., 2018. Patient-specific CFD modelling in the thoracic aorta with pc-mri-based boundary conditions: A least-square three-element windkessel approach. *Int. J. Numer. Methods Biomed. Eng.* <https://doi.org/10.1002/cnm.3134>.
- Sigovan, M., Hope, M.D., Dyverfeldt, P., Saloner, D., 2011. Comparison of Four-Dimensional Flow Parameters for Quantification of Flow Eccentricity in the Ascending Aorta. *J. Mag. Res. Imag.* 34, 1226–1230.
- Simao, M., Ferreira, J.M., Tomas, A.C., Fragata, J., Ramos, H.M., 2017. Aorta Ascending Aneurysm Analysis Using CFD Models towards Possible Anomalies. *Fluids* 2, 1–15.
- Steinman, D.A., 2012. Assumptions in modelling of large artery hemodynamics. Springer, Milano.
- Stevens, R.R.F., Grytsan, A., Biasetti, J., Roy, J., Liljeqvist, M.L., Gasser, T.C., 2017. Biomechanical changes during abdominal aortic aneurysm growth. *PLoS ONE*. <https://doi.org/10.1371/journal.pone.0187421>.
- Stonebridge, P.A., Hoskins, P.R., Allan, P.L., Belch, J.F., 1996. Spiral laminar flow in vivo. *Clin. Sci.* 91, 17–21.
- Tarbell, J.M., 2003. Mass transport in arteries and the localization of atherosclerosis. *Annu. Rev. Biomed. Eng.* 5, 79–118.
- Torii, R., Keegan, J., Wood, N.B., Dowsey, A.W., Hughes, A.D., Yang, G.-Z., Firmin, D.N., Thom, A.M., Xu, X.Y., 2009. The effect of dynamic vessel motion on haemodynamic parameters in the right coronary artery: a combined MR and CFD study. *Brit. J. Radiol.* 82, S24–S32.
- Weigang, E., Kari, F.A., Beyersdorf, F., Luehr, M., Etz, C.D., Frydrychowicz, A., Harloff, A., Markl, M., 2008. Flow-sensitive four-dimensional magnetic resonance imaging: flow patterns in ascending aortic aneurysms. *Euro. J. Cardio. Thora. Surg.* 34, 11–16.
- Youssefi, P., Gomez, A., Arthurs, C., Sharma, R., Jahangiri, M., Figueroa, C.A., 2018. Impact of patient-specific inflow velocity profile on hemodynamics of the thoracic aorta. *J. Biomech. Eng.* 140, 011002–1 – 011002–14.
- Yu, S.C., Liu, W., Wong, R.H., Underwood, M., Wang, D., 2016. The Potential of Computational Fluid Dynamics Simulation on Serial Monitoring of Hemodynamic Change in Type B Aortic Dissection. *Cardiovasc. Intervent. Radiol.* 39, 1090–1098.